Aminoglycoside−Arginine Conjugates That Bind TAR RNA: Synthesis, Characterization, and Antiviral Activity†

Alexander Litovchick,‡ Artem G. Evdokimov,§ and Aviva Lapidot*,‡

Departments of Organic Chemistry and Structural Biology, The Weizmann Institute of Science, 76100 Rehovot, Israel

Received August 2, 1999; Revised Manuscript Received November 10, 1999

ABSTRACT: Regulation of HIV gene expression is crucially dependent on binding of the trans-activator protein, Tat, to the trans-activation response RNA element, TAR, found at the 5′ end of all HIV-1 transcripts. Tat−TAR interaction is mediated by a short arginine-rich domain of the protein. Disruption of this interaction could, in theory, create a state of complete viral latency. A new class of small-molecule peptidomimetic TAR RNA binders, conjugates of aminoglycosides and arginine, was recently designed [Litovchick, A., Evdokimov, A. G., and Lapidot, A. (1999) *FEBS Lett. 445*, 73−79]. Two of these compounds, the tri-arginine derivative of gentamicin C (R3G) and the tetra-arginine derivative of kanamycin A (R4K), bind efficiently and specifically to TAR RNA. These compounds display negligible toxicity while being transported and accumulated in cell nuclei. Here we present a detailed synthesis and chemical characterization of the aminoglycoside−arginine conjugates R3G and R4K as well as GB4K, the tetra-γ-guanidinobutyric derivative of kanamycin A. Their binding sites on TAR RNA were assigned by RNase A, uranyl nitrate, and lead acetate footprinting. The conjugates interact with TAR RNA in the widened major groove, formed by the UCU bulge and the neighboring base pairs of the upper stem portion of TAR, the binding site of Tat protein, and Tat-derived peptides (e.g., R52). Our results suggest an additional binding site of R4K and R3G compounds, in the lower stem−bulge region of TAR. The antiviral activity of the conjugates in cultured equine dermal fibroblasts infected with equine infectious anemia virus, used as a model system of HIV-infected cells, is also presented.

The trans-activation responsive RNA (TAR)[1] region of HIV long terminal repeat (LTR) regulates the viral gene expression via interaction with the HIV trans-activator protein, Tat, and thus is an attractive target for drug design strategies *(1)*. TAR is found at the 5′ end of all HIV-1 transcripts. It adopts a hairpin secondary structure consisting of a highly conservative hexanucleotide loop and a three-nucleotide bulge flanked by two double-stranded stems (*2*). TAR is a positive enhancer that stimulates the synthesis of productive transcripts. It is unique in terms of eukaryotic transcription control because it only functions as an RNA element. The activation by Tat is entirely dependent on the presence of the TAR RNA sequence. Tat activates expression by specific binding to TAR, which increases viral mRNA production several hundredfold by stimulation of the elongation capacity of RNA polymerase II *(3)*. HIV Tat binds the cyclin T subunit of P-TEFb and recruits P-TEFb to the HIV-1 LTR promoter. This process requires binding of Tat to the TAR bulge and of cyclin T to the TAR loop. The cyclin T-associated CDK9 kinase then induces phosphorylation of the C-terminal domain of RNA polymerase II, and of other polymerase II-associated proteins, leading to the transition from nonprocessive to processive transcription *(4)*.

Binding of Tat protein to TAR is mediated by the nine amino acid region RKKRRQRRR (residues 49−57) of the protein *(5−12)*. The nona-arginine peptide (R_9) binds to TAR with the same affinity and specificity as the wild-type Tat peptide, whereas the nona-lysine peptide (K_9) binds to TAR nonspecifically and with a 10-fold lower affinity. The R_9-containing Tat mutant protein gives wild-type trans-activation activity and is 100 times more active than the K_9-containing protein. Insertion of a single arginine moiety at position 52 or 53 (R52 or R53 peptides) restores RNA-binding affinity and specificity of the peptide as well as its trans-activation potency *(2)*. Mutagenesis studies on TAR RNA demonstrated

† This work was supported in part by research grants from Yeda Research Co. (WIS) and the Israeli Ministry of Science to A.L. A.L. is an incumbant of the Lee and William Abramovitz Professorial Chair of Macromolecular Biophysics.

* To whom correspondence should be addressed at the Department of Organic Chemistry, The Weizmann Institute of Science. Tel: 972-8-9343413; Fax: 972-8-9344142. Email: aviva.lapidot@weizmann.ac.il.

‡ Department of Organic Chemistry.

§ Department of Structural Biology.

[1] Abbreviations: AAC, aminoglycoside−arginine conjugate; HIV, human immunodeficiency virus; AIDS, acquired immunodeficiency syndrome; TAR, trans-activation responsive element; LTR, long terminal repeat; P-TEFb, positive transcription elongation factor b; Tat, trans-activator of transcription; CDK9, cyclin-dependent kinase; BIV, bovine immunodeficiency virus; EDTA, ethylenediaminetetraacetic acid; RRE, Rev response element; R3G, tri-arginine−gentamicin C conjugate; R4K, tetra-arginine−kanamycin A conjugate; GB4K tetra-γ-guanidinobutyric acid−kanamycin A conjugate; DMF, dimethylformamide; DCC, *N*,*N*′-dicyclohexylcarbodiimide; TFA, trifluoroacetic acid; FABHRMS, fast-atom bombardment high-resolution mass spectroscopy; ED, equine dermal fibroblasts; EIAV, equine infectious anemia virus; DMEM, Dulbecco modified Eagle medium; FCS, fetal calf serum; FITC, fluorescein isothiocyanate; HSQC, heteronuclear single-quantum coherence; TOCSY, total coherence spectroscopy; pfu, plaque forming unit; cpe, cytopathic effect; HEPES, *N*-(2-hydroxyethylpiperazine)-*N*′-2-ethanesulfonic acid; SDF-1α, stromal cell-derived factor 1α; CXCR4, CXC (chemotactic cytokines related to interleukin-8) chemokine receptor 4.

10.1021/bi9917885 CCC: $19.00
Published on Web 02/24/2000

that the bulge (U23-C24-U25) and two base pairs on both sides of the bulge *(5, 6, 13−15)* are important for Tat binding. Full-length Tat protein binds TAR with only moderate affinity and specificity in vitro. The first 37 N-terminal amino acids of the Tat protein decrease its affinity to TAR in comparison to the specific recognition Tat (38−72) peptide *(16)*. It was shown that human cyclin T1 promotes cooperative binding of Tat protein to TAR RNA in vitro and mediates trans-activation in vivo. Although cyclin T1 does not bind TAR RNA, it may interact with the TAR loop in a ternary complex of cyclin T1−Tat−TAR *(17)*.

NMR structures of HIV TAR and bovine immunodeficiency virus (BIV) TAR bound to different ligands, e.g., as peptides that mimic the basic region of Tat, arginine and argininamide, show that the ligands bind to the TAR RNA major groove *(18−24)*. The bulge structure allows ligands to access the major groove of TAR, which induces folding in the bulge and formation of unusual base-triples *(18−24)*. The TAR RNA hairpin can adopt two major conformations. In the absence of ligands, the bulge nucleotides stack within the RNA stem, severely distorting its helical continuity *(18, 23)*. When either L-argininamide or the Tat peptide bind to TAR, the bulge nucleotides loop out of the remaining stem, allowing the upper and the lower stem helices to stack coaxially *(18, 22, 24)*. The NMR structure of L-argininamide bound to TAR suggests proximity between the bulge and apical loop across the RNA major groove *(23)*. The specific interactions between HIV Tat protein and TAR RNA are still unknown but could be modeled as a basic α-helix of Tat peptide lying in the major groove of TAR *(25, 26)*. BIV Tat recognition domain (17-mer) folds into a *β*-hairpin and penetrates into a widened major groove of the 28-mer BIV TAR RNA in an edge-on orientation *(20, 22)*. Proximity probing by affinity cleavage, using Tat peptide conjugate to Fe(II)-EDTA, suggests that the formation of Tat−TAR complex brings the loop of the RNA in the vicinity of the bulge *(16, 27)*, a suggestion which is strongly supported by the NMR model. RNA self-cleavage experiments, using a covalently attached EDTA analogue at U24 of TAR (the wild-type TAR contains C24 instead), confirm the binding of Tat peptide in the bulge and demonstrate that U24-EDTA is rigidly positioned out of the helix *(16, 28)*.

Tat-derived basic peptides as well as the oligocationic peptide and peptoid Tat mimetics bind TAR RNA with high affinity in vitro *(5−12, 29−32)*. Tat-mimetic compounds ALX40-4C *(29)* and CGP64222 *(30)*, that target TAR RNA, demonstrate a pronounced antiviral activity. D-Tat peptide, derived from the Tat 37−72 sequence, is another candidate for pharmaceutical applications. It binds to the TAR RNA major groove and interferes with the transcriptional activation by Tat protein in vitro and in HeLa cells *(32)*.

Aminoglycosides not only bind to hairpin structures on 16S RNA *(33−35)* but also bind to HIV TAR, as well as Rev responsive element (RRE) RNA *(36−39)*. A wide variety of aminoglycosides inhibit Tat binding to TAR at a millimolar range of concentration *(37)*. Neomycin B was reported as a specific inhibitor of Rev−RRE interaction *(36)*. It was also found to be the most efficient aminoglycoside TAR RNA binder *(37)*. It was shown that neomycin B noncompetitively inhibits Tat−TAR interaction in vitro in the range of 0.1−1 mM *(38)*. The binding site of neomycin B is located in the lower stem and the bulge of TAR RNA, as was determined by footprinting studies *(38, 39)*. Its binding, however, is not affected by introduction of mutations in the UCU bulge *(37)*. Computer docking and molecular dynamics simulations predict the recognition of this antibiotic by G21−C41 and A22−U40 pairs, as well as U23 and G26 nucleotides of TAR RNA *(40)*.

Metal ions play an important role in stabilizing a variety of RNA structural motifs by forming both inner-sphere and outer-sphere (through water) interactions with RNA functional groups. Mg^{2+} ions are required for folding and function of hammerhead ribozyme *(41, 42)*. It was shown that aminoglycosides, upon binding to this ribozyme, replace magnesium ions *(43)*. TAR RNA may also bind divalent metal ions (such as Ca^{2+}), as was found in the X-ray structure of model TAR *(44)*. These data are supported by hydrodynamic studies of the influence of metal ion (Mg^{2+}) binding on TAR RNA bulge region conformation *(44−46)*. It is possible that the TAR-bound ligands interact in some way with the metal ions in the bulge region, though the arginine affinity to TAR is not altered by magnesium ions *(46)*.

Based on peptide models of TAR RNA binding, NMR structures of TAR−ligand complexes, and aminoglycoside−RNA interactions, we recently designed and synthesized a set of novel peptidomimetic substances, conjugates of aminoglycoside antibiotics with arginine *(47*, Figure 1). The combination of arginine residues and an aminoglycoside core results in new compounds with structural features of both the oligocationic peptides and the aminoglycosides. These aminoglycoside−arginine conjugates (AAC) display high affinity to TAR RNA in vitro: K_d's of AAC−TAR complexes measured by the gel-shift technique were found to be in the range of 20−400 nM *(47)*, comparable to the K_d of the native Tat−TAR complex (6−12 nM). The finding that gel-electrophoretic mobilities of the AAC−TAR differ from peptide−TAR complexes suggests that the stoichiometry of the complex between AAC and TAR RNA in vitro is not equimolar.

Aminoglycoside−arginine conjugates are nontoxic for cultured mammalian cells. Fluorescently labeled AAC efficiently accumulate in mammalian cell nuclei as was determined by confocal fluorescent microscopy studies *(47)*. AAC are expected to be resistant to enzymatic degradation that comprises one of the main problems for peptide therapies.

In this report, we describe a detailed synthesis and chemical characterization of three conjugates, footprinting analysis of their binding to TAR RNA, and also their antiviral activity.

EXPERIMENTAL PROCEDURES

Synthesis of Aminoglycoside Conjugates (48, Figure 2). Method 1. Aminoglycoside−arginine conjugates were prepared using the following procedure: 1−10 mmol of an aminoglycoside antibiotic (kanamycin A or gentamicin C, Fluka) was dissolved in 30 cm^3 of an anhydrous DMF/pyridine mixture (8:1). For each amino group of the aminoglycoside, 1.1 equiv of N^{α}-carbobenzoxy-N^{ω}-nitroarginine (Sigma) and 1.15 equiv of *N*,*N*′-dicyclohexyl carbodiimide (DCC, Merck) were added in 4−6 portions during 24−48 h. The reaction was allowed to proceed for another 32 h at room temperature. Precipitated *N*,*N*′-dicyclohexylurea was

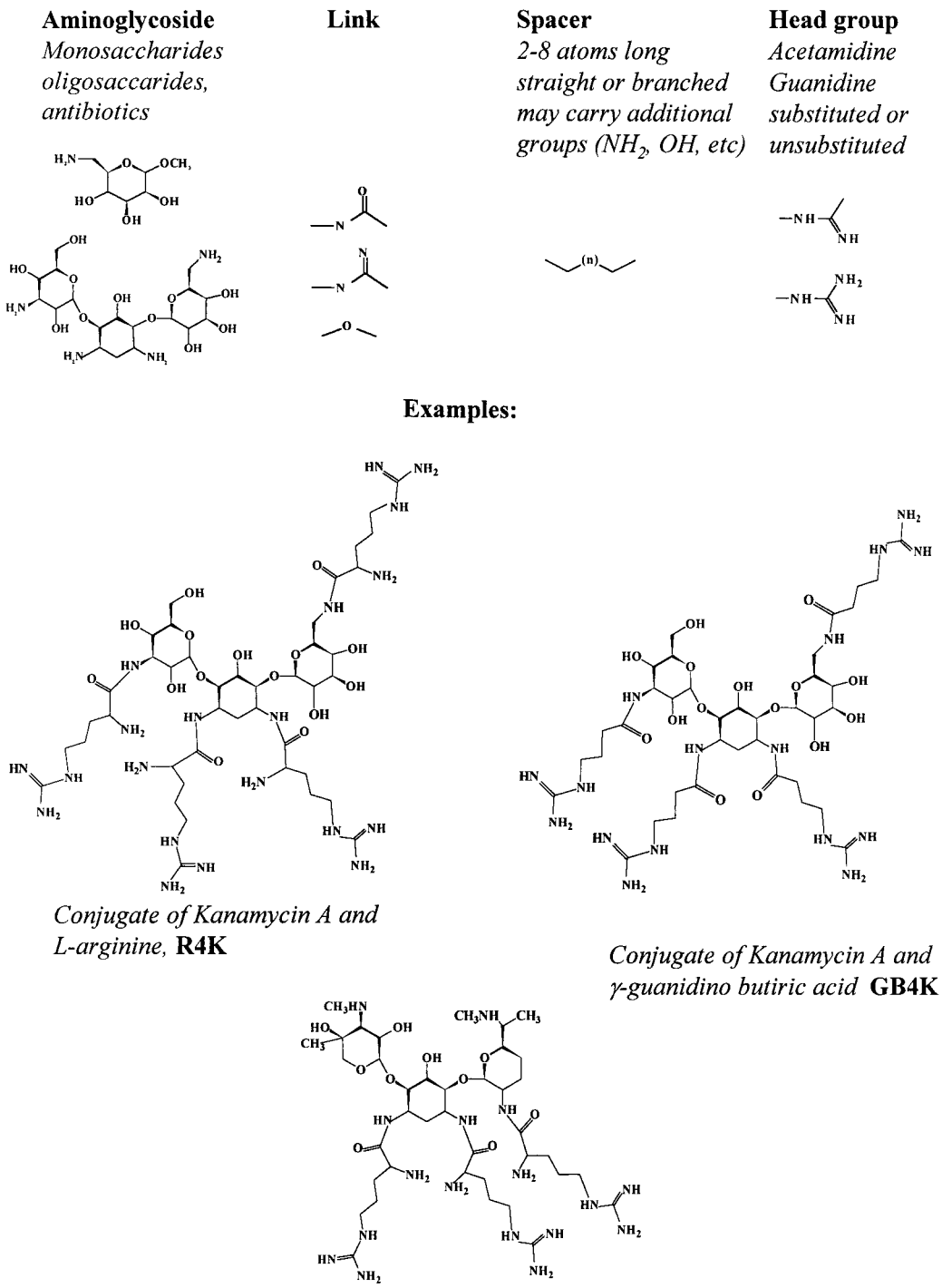

FIGURE 1: Peptidomimetic design overview. Aminoglycoside-based peptidomimetic substances visualized as combinations of the oligosaccharide core linked to several side chains bearing charged headgroups (guanidino or acetamidino). Conjugates of aminoglycoside antibiotics (kanamycin A and gentamicin C) with arginine and γ-guanidinobutyric acid are shown.

removed by filtration, the filtrate was evaporated in vacuo, and the residue was washed with water and chloroform. After lyophilization, the residue was dissolved in an alcohol/dioxane mixture (1:1) containing 1−1.5 equiv of acetic acid per each protected charged group (based on the theoretical yield), and hydrogenated at atmospheric pressure for 12−20 h over 0.5 g of 10% Pd/charcoal catalyst. After this treatment, the substances gained solubility in water. The solvents were evaporated in vacuo, and the residue was dissolved in water (or a water/alcohol mixture), a fresh portion of acetic acid was added, and the hydrogenation was continued for another 24 h. The catalyst was removed by centrifugation, and the solution was evaporated in vacuo, resulting in faintly yellow, viscous syrup, which was then dissolved in 15 cm^3 of water. This solution was passed through a Dowex 1x8 (OH^-) column, to remove the acetic acid and free arginine. The eluted solution was loaded onto an Amberlite IRC-50 (H^+), and the column was successively washed with deionized water, 5 N ammonia, and water. The column was eluted with 0.5 M HCl, neutral fractions were collected and evaporated to dryness, and the solid residue was extracted with 95% alcohol. Extracts were evaporated

and dissolved in 15 cm^3 of water, and the solution was passed again through Dowex 1x8 (OH^-) and evaporated to dryness, resulting in 100−300 mg of glassy solid of the desired conjugate with 85−90% purity (overall yield 10−15%). For higher purity, the crude conjugate was applied onto a 10 × 250 mm HiBar column (C-18 Merck) and chromatographed in a 40 min gradient from 0 to 40% acetonitrile/0.1% trifluoroacetic acid (TFA) at 2.5 mL/min. Peaks of interests were eluted at 22.5−27.5 min. The TFA salts of the conjugates were used only for in vitro studies; free base conjugates were utilized in the cell culture experiments, due to significant toxicity of the TFA anion.

Method 2. Four equivalents of *N*-hydroxysuccinimide ester of N^{α}-*tert*-butoxycarbonyl-N^{ω}-carbobenzoxy-L-ornithine was coupled to 1 equiv of kanamycin A free base in a water/alcohol/dioxane mixture for 12 h. The reaction mixture was then evaporated, the residue was washed with deionized water, and the carbobenzoxy protective groups were subsequently removed by hydrogenation, as described under Method 1. The resulting conjugate of N^{α}-*tert*-butoxycarbonyl-L-ornithine with kanamycin A was treated with 12−15 equiv of *S*-methylisothiourea sulfate in 5% aqueous ammonia for 3−5 days. The resulting conjugate of N^{α}-*tert*-butoxycarbonyl-L-arginine with kanamycin A was deprotected in 100% TFA in the presence of 10 equiv of dimethyl sulfide for 8 h at room temperature. The further purification of R4K was performed as in Method 1 (overall yield 25−35%).

γ-Guanidinobutyric acid−kanamycin A conjugate (GB4K) was prepared by the following procedure: 4 equiv of *N*-hydroxysuccinimide ester of *N*-carbobenzoxy-γ-aminobutyric acid (GABA) was coupled to 1 equiv of kanamycin A free base in a water/alcohol/dioxane mixture for 12 h. The reaction mixture was treated as described above, and the carbobenzoxy protecting group was removed by hydrogenation. The resulting conjugate of GABA with kanamycin A was treated with an excess of *S*-methylisothiourea sulfate in 5% ammonia solution. The resulting GB4K was purified by the same ion-exchange chromatography procedure as described for the aminoglycoside−arginine conjugates. The overall yield was 15−25%, and the purity after ion-exchange chromatography was 90−95%. The compound was used without any further purification.

The final products were characterized by FAB high-resolution mass spectroscopy (FABHRMS) and by ^1H and ^{13}C NMR (Bruker AMX 400 MHz).

RNA and Peptide Preparation. A 31 nucleotide TAR RNA fragment (5′-GGC CAG AUC UGA GCC UGG GAG CUC UCU GGC C-3′) containing sequence 18−44 of HIV-1 LTR was synthesized by Dharmacon Inc. by means of phosphoamidate chemistry. Dharmacon RNA crude products are typically >90% pure; after HPLC or/and gel purification, the purity could be increased to >99%. The chemistry employs a 5′-silyl protecting group in conjunction with a unique acid-labile 2′-ortho ester protecting group, 2′-bis-(acetoxyethoxy) methyl ether (2′-ACE) *(49)*. The 2′-ACE protection at 2′-OH was removed using the company's protocol and buffer. The RNA was 5′-end-labeled with 1 μL of [γ-^{32}P]ATP (6000 Ci/mmol, Amersham) per 1 nmol of RNA using T4 polynucleotide kinase (Promega) in a buffer containing 70 mM Tris-HCl, pH 7.5, 10 mM $MgCl_2$, and 5 mM DTT. The labeled RNA was successively extracted with water-saturated phenol, phenol/chloroform (1:1), and chloroform, and precipitated from 75% ethanol. All RNA samples were annealed by heating them to 95 °C for 5 min, followed by slow-cooling to room temperature in a buffer containing 10 mM sodium cacodylate (pH 6.5) and 50 mM KCl. RNA purity was analyzed by denaturing gel electrophoresis. Binding of TAR RNA to Tat R52 and conjugates was tested by gel-shifts *(47)*. Binding competition was performed in the presence of yeast tRNA ("Sigma"). Results were visualized by exposing the wet gels to Fuji phosphoimager plates, which were read on a "Storm 820" (Molecular Dynamics) phosphoimager. The alkaline cleavage of TAR RNA was performed by incubation of 10 μL RNA samples (containing 50−100 ng of 5′-^{32}P-labeled TAR RNA) with 10 mM NaOH for 3−5 min at room temperature. The reaction was stopped by addition of 1 μL of 150 mM acetic acid.

The model Tat peptide R52 (YKKKRKKKKKA) *(2)* was prepared by the Weizmann Institute Chemical Service and was purified by reverse-phase HPLC (C18) *(47)*.

RNase A Footprinting. In a typical experiment, 10 μL of 5 mM cacodylate buffer, pH 6.5, containing 25 mM KCl and 50−100 ng of 5′-^{32}P-labeled TAR RNA (approximately 0.5−1 μM) was incubated with 200 pM RNase A (Sigma) at room temperature for 10 min in the presence of Tat R52 and the conjugates at various concentrations. In the competition experiments, the mixture was supplemented with 0.5 μg of yeast tRNA (Sigma). After the incubation, 10 μL of formamide/bromphenol blue loading buffer was added to the samples. The samples were heated to 80 °C for 2 min and were resolved by electrophoresis on a 40 cm × 0.8 mm 20% polyacrylamide denaturing gel (7M urea) for 3 h at 55 °C. The results were visualized by a phosphoimager as described above and quantitated using ImageQuant software.

Lead Acetate Footprinting. In a typical experiment, 10 μL of 50 mM cacodylate buffer, pH 6.5, containing 100 mM KCl, 1 mM $MgCl_2$, and 0.5 μg of yeast tRNA was incubated with 50 ng of 5′-^{32}P-labeled TAR RNA (approximately 0.5 μM) in the presence of varying concentrations of Tat R52 and AAC at room temperature for 5 min. Cleavage reactions were initiated by addition of $Pb(OAc)_2$ to final concentrations of 0.1 mM. After 20 min incubation, 10 μL of 90% formamide/bromphenol blue loading buffer, containing 100 mM EDTA, was added to the samples. The samples were heated to 80 °C for 2 min and were resolved by electrophoresis and quantitated as described above.

Uranyl Nitrate Photocleavage. The procedure for photoinduced cleavage of TAR RNA by uranyl cation was as follows: 50 μM uranyl nitrate was added to 10 μL of 5 mM cacodylate buffer, pH 6.5, or 5 mM KMOPS buffer, pH 7.5, containing 25 mM KCl and 1 μM 5′-^{32}P-labeled TAR RNA. Inhibitors or divalent metal salts were added to the mixture at various concentrations. Tracing of the hypersensitive cleavage sites was performed in the presence of 37.5 μM citrate. The samples were irradiated for 10−20 min at room temperature under a Philips T1 40 W/03 fluorescent tube, emitting light at a wavelength of 420 nm. Following irradiation, the samples were treated, resolved by electrophoresis, and quantitated as described above.

Antiviral Activity in Cell Culture. Both equine dermal fibroblasts (ED) and equine infectious anemia virus (EIAV), Wyoming isolate, adapted to growth in fibroblasts (Malmquist virus) *(50)* were gifts from Profs. A. Yaniv and A.

Gazit, from the Sackler Medical School of Tel-Aviv University. ED cells were plated on plastic 6-well tissue culture plates (Nunclone) at a density of 5×10^5 cells per well in 2 mL of DMEM/10% FCS (fetal calf serum). The medium was removed after 12−20 h, and the cells were inoculated for 2 h with 0.5 mL of DMEM/10% FCS containing 5×10^6 pfu (plaque-forming units) of EIAV and 10 μg/mL Polybrene (hexadimetrine bromide, Sigma) *(51)*. Following the incubation, another 2.5 mL of DMEM/10% FCS was added to each well. On the following day, the medium was discarded and was substituted for 2 mL of DMEM/10% FCS, containing 0.5 μCi/mL [5,6-^{3}H]uridine (Amersham). Different concentrations of the conjugates were added to the wells, in duplicate. Every 3−4 days, 1.2 mL samples of the medium were collected and replaced with the same amount of medium, containing radioactive uridine and the tested compounds. The samples were clarified from cell debris by spinning at 12 000 rpm for 5 min on the Eppendorf centrifuge. Viral particles from the clarified supernatants were collected by ultracentrifugation at 75 000 rpm, 4 °C, on the Beckman TL 100 centrifuge using a TLA 100.2 rotor *(52)*. The supernatants were carefully discarded, and the pellet was resuspended in 200 μL of 1% SDS/5% Triton X-100, mixed with 1 mL of Ultima Gold scintillation liquid (Packard), and counted by an LS 1701 Bruker scintillation counter. The quantitation of the viral production, as described above, was compared with the reverse transcriptase assay *(51)* performed on the viral pellets. Results obtained by both methods correlate well, so the simpler one was applied as described above. The typical duration of the experiment was 15 days; EIAV growth curves in the presence of various concentrations of R4K, R3G, or GB4K in the medium were obtained. Development of the cytopathic effect in the infected ED cells was monitored by light microscopy.

Cellular Uptake into Infected Cells Using Fluorescent Probes. The fluorescent derivatives of R4K and R3G were prepared by reacting free-base conjugates with fluorescein isothiocyanate (FITC, Sigma) in a water/methanol/DMSO mixture as described previously *(47)*. EIAV-infected ED cells at the late stage of infection were plated on collagen-coated glass slides and incubated in HEPES-buffered saline in the presence of 10 μg/mL FITC-labeled compounds for 0.5−1 h. The slides were washed several times with saline and studied by confocal laser-scanning microscopy on the Axiovert 100M (Zeiss) microscope, using 488 nm excitation (argon-ion laser) and 505−550 nm emission band.

RESULTS

Chemical Characterization of the Aminoglycoside Conjugates. R4K was characterized as a free base and comprised, according to HPLC, of essentially one product, the kanamycin A derivative (Figure 2). The ^{1}H NMR (400 MHz, D_2O) spectrum revealed the presence of the characteristic groups of the protons of arginine amide moieties at chemical shifts of (δ) 3.38 (H_α), 3.21 (H_β), and 1.64 ppm ($H_{\gamma,\delta}$). All the characteristic kanamycin proton signals, in particular the anomeric hydrogens (as doublets at 4.99 and 5.15 ppm), were observed. Integration afforded a 1:4 ratio of antibiotic to arginine components. A ^{13}C NMR (100 609 MHz 10% D_2O) spectrum of R4K revealed carbon resonances of the C-arginine amide moieties and the kanamycin moiety. The

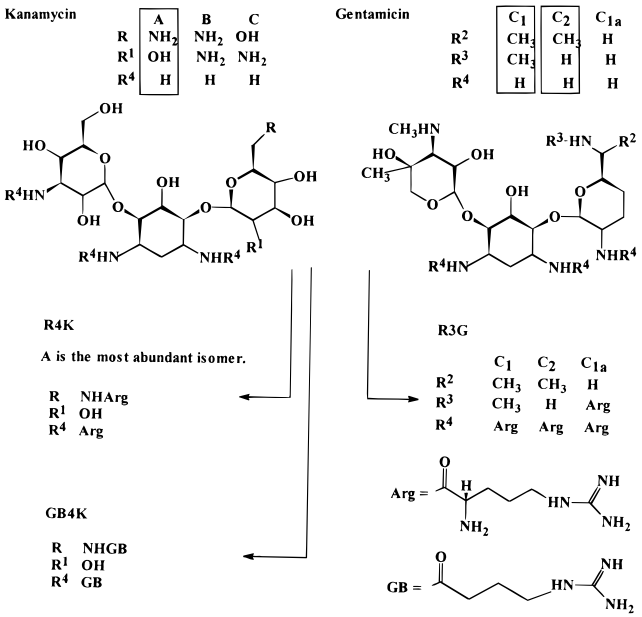

FIGURE 2: Scheme of synthesis of tetra-arginine−kanamycin A conjugate (R4K), tetra-γ-guanidinobutyric acid−kanamycin A conjugate (GB4K), and tri-arginine−gentamicin C conjugate (R3G).

presence of antibiotic anomeric carbon signals at 101.77 and 101.07 ppm, the amide carbons at 181.13, 180.81, 180.38, and 179.76 ppm, and the guanidino carbons at 159.47 ppm confirmed the structure of the aminoglycoside−arginine conjugate. FABHRMS of R4K revealed a mass peak of 1109.7 Da (calculated molecular mass of R4K, 1109.25 Da). A second peak of 1067.4 Da (−42.3 Da from the mass peak) was attributed to a loss of an iminoamino carbon fragment during ionization.

R3G was characterized as an acetate salt (at pH 7.0). The substance is a mixture of three products (as was proved by analytical HPLC), the derivatives of gentamicin C isomers (C_1, C_2, and C_{1a}), differing by methylation of a single amino group and adjacent CH_2 *(53*, Figure 2). Since the structural difference between the three components is minor, the substance was used as a mixture in this study. Characteristic arginine amide ^{1}H NMR resonances of R3G were observed at ca. 3.4 (H_α), 3.2 (H_β), and 1.6 ($H_{\gamma,\delta}$) ppm and characteristic antibiotic proton resonances, in particular the anomeric hydrogens, as three groups of doublets at 5.0−5.35 ppm; methyl singlets at 2.51 (N-Me of C_1, C_2, and C_{1a} isomers), 2.32 (N-Me of C_1), and 1.21 (C-Me of C_1, C_2, and C_{1a}) ppm; and methyl multiplet at 1.04 ppm (N-Me of C_1, C_2). Integration afforded a 1:3 average ratio of the gentamicin C components to arginine components, based on the composition of the antibiotic mixture used for the synthesis. A ^{13}C NMR spectrum revealed carbon resonances at several distinct regions characteristic of C-arginine amide moieties and three gentamicin isomeric moieties. Several C-amide carbon signals at 179.8−179.3 ppm were observed as two groups of three peaks, as well as several minor peaks, indicating the presence of two major isomers, as suggested by the composition of the original antibiotic mixture. Guanidino carbon signals were detected at 160.04 ppm. FABHRMS of R3G revealed two prominent mass peaks of 948.3 and 934.3 Da (calculated masses of 948.1 and 934.1 Da), which correspond to the tri-arginine derivatives of C_1 and C_2 isomers, differing by a methyl group. Loss of the iminoamino

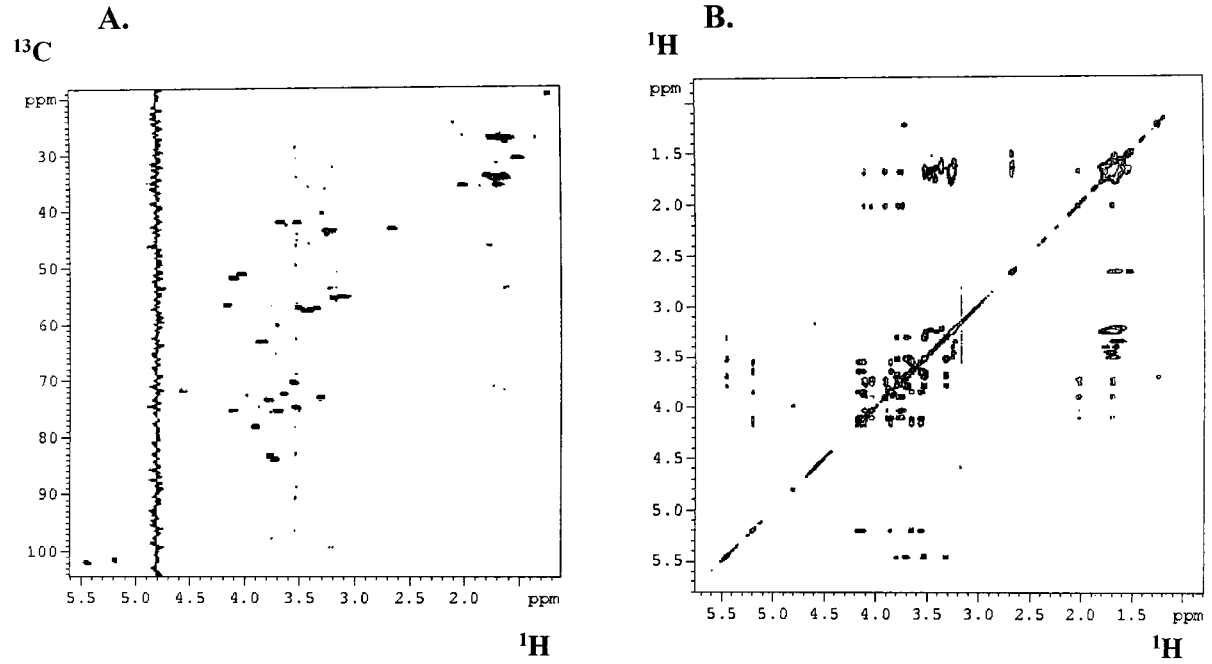

FIGURE 3: 2D NMR spectra of R4K. The spectra were recorded on Bruker DPX 500 MHz at 21 °C in D_2O. (A) [^{1}H; ^{13}C] natural abundance heteronuclear single-quantum coherence (HSQC). Characteristic cross-peaks, in particular from the two anomeric proton signals of the two saccharide rings at 4.99 and 5.15 ppm with corresponding carbon signals at 101.1 and 101.8 ppm, are observed. (B) Total coherence spectroscopy (TOCSY) was acquired at 120 ms mixing time. Cross-peaks with ring anomeric protons at 5.2 and 5.4 ppm allow assignment of the two sugar rings of the antibiotic. Correlations of deoxystreptamine axial and equatorial methylene protons (1.65 and 1.92 ppm) with the deoxystreptamine ring system are observed. Methylene protons at C_γ and C_δ of arginine amide moieties (1.6−1.8 ppm) correlate with protons at C_β (3.25−3.45 ppm).

carbon fragment on chemical ionization by FABHRMS was also visible.

GB4K was characterized as an acetate salt. Characteristic ^{1}H signals of guanidinobutyric acid amide chains were observed as multiplets at 3.19 (H_α), 2.32 (H_β), and 1.86 ($H_{\gamma,\delta}$) ppm. All characteristic signals of the kanamycin moiety were found, in particular the anomeric protons as singlets at 5.32 and 5.11 ppm. Integration afforded a 1:4 ratio of the antibiotic to guanidinobutyric acid amide parts. A ^{13}C NMR spectrum revealed characteristic groups of signals of both the guanidinobutyric acid amide and the antibiotic moiety. In particular, the antibiotic anomeric carbon signals were observed at 100.03 and 98.04 ppm; the amide carbons at 176.63, 176.22, 175.32, and 174.94 ppm; and the guanidino carbons at 157.33 ppm. Using FABHRMS, the mass peak was found to be 993.5 Da (calculated 993.1 Da). Loss of the iminoamino carbon fragment upon ionization was also observed.

2D NMR Studies of Kanamycin A−Arginine Conjugate R4K. Since R4K was comprised of essentially one substance, it was suitable for 2D NMR studies. Natural abundance [^{1}H; ^{13}C] heteronuclear single-quantum coherence (HSQC) and total correlation spectroscopy (TOCSY) *(54)* spectra of R4K were recorded on a Bruker DPX 500 MHz in D_2O at 21 °C.

HSQC reveals the characteristic proton and carbon signal cross-peaks, in particular from the two anomeric protons of the two saccharide rings (4.99 and 5.15 ppm) with corresponding carbons (101.1 and 101.8 ppm) (Figure 3 A). TOCSY of R4K was acquired at 120 ms mixing time. The spectrum reveals two sugar rings of the antibiotic emphasized by correlation with their anomeric protons at 5.2 and 5.4 ppm. Correlations between the deoxystreptamine axial and equatorial methylene protons (1.65 and 1.92 ppm) and the ring system are observed. Methylene protons at C_γ and C_δ of arginine amide moieties (1.6−1.8 ppm) display correlation with the protons at C_β (3.25−3.45), and it is possible to observe four arginine side chains (Figure 3B). Both spectra contributed much to the correct assignment of the R4K proton and carbon resonances.

Determination of the AAC Binding Sites on TAR RNA by RNase A Footprinting (Figure 4A). TAR RNA and RNase A concentrations were established by cotitration. To produce "single-hit" kinetic conditions *(55)*, 1 μM TAR versus 200 pM RNase A was selected. Tat R52 and AAC concentrations were determined by titration. Effective protection of 1 μM TAR was observed with 2 μM Tat R52, 10 μM R4K, and 4 μM R3G. GB4K did not exhibit binding to TAR RNA, neither in gel-shift experiments (up to 50 μM) nor in the protection experiments (at 40 μM). RNase A cleaved TAR RNA in an uneven manner (Figure 4A, lane 2). The most susceptible regions for cleavage were the single-stranded loop, nucleotides U31−G34, as well as C24 and U25 of the bulge. Strong cleavage was also observed at G21−G41 and A20−U42 pairs (lower stem). Binding of R52 (2−4 μM) caused a weakening of the bands in the upper stem region (G26−C39, A27−C38, as well as U40) (Figure 4A, lanes 3, 4*)*. At 4 μM R52, the cleavage at G34 (loop) was enhanced, as well as a certain enhancement of bands A20, G21, U23, and U25 was observed. Remarkably, the band corresponding to the R52−TAR complex still was observed on the gels even after electrophoresis under strongly denaturing conditions. In the presence of R4K (10−20 μM), the upper stem (G26−C29), the lower stem, and the bulge (G21−U23, partially C24 and U25) were protected as well as C38, C39, and U40. Cleavage at C19 and A20 of the lower stem and C30, G33, and G34 of the loop was enhanced by 10 μM R4K, whereas with 20 μM R4K the protection of

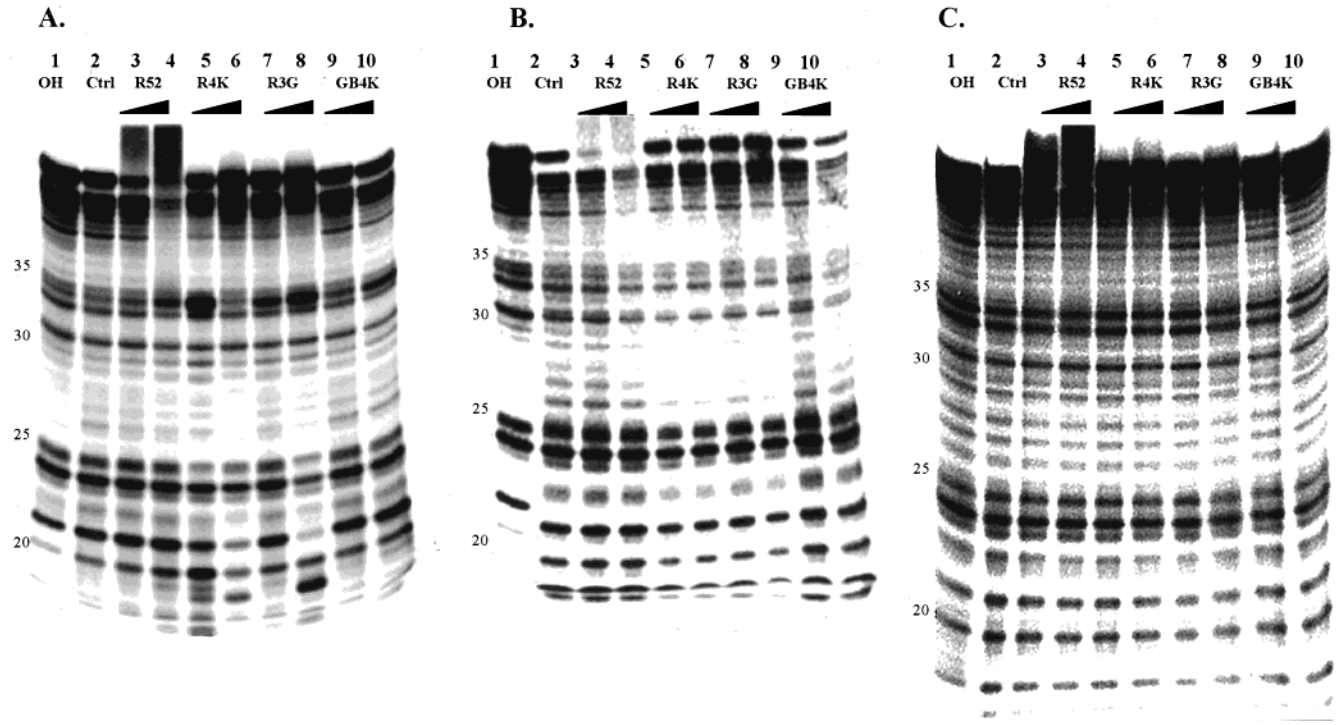

FIGURE 4: Footprinting studies of the binding sites of aminoglycoside−arginine conjugates on TAR RNA. Approximately 100 nM 5′-^{32}P end-labeled TAR was used per lane. Lane "OH" represents alkaline hydrolysis of TAR. Concentrations of Tat R52 peptide, 2−4 μM (lanes 3, 4); R4K, 10−20 μM (lanes 5, 6); R3G, 4−8 μM (lanes 7, 8); GB4K, 20−40 μM (lanes 9, 10) (see Experimental Procedures). (A) RNase A footprinting. Lane "Ctrl" represents RNase cleavage in the absence of binders. (B) Uranyl photocleavage. The reactions were performed in cacodylate buffer, pH 6.5 (slightly acidic conditions modulate the uranyl cleavage, reflecting the conformational changes of nucleic acids). The samples were irradiated for 10 min at 420 nm. Lane "Ctrl" represents uranyl photocleavage in the absence of binders. (C) Lead acetate footprinting. Lane "Ctrl" represents lead acetate cleavage in the absence of binders. The gels were analyzed using a Storm 820 phosphoimager; quantitations were obtained using the ImageQuant program.

C30, G34, and A20−G21 was observed (Figure 4A, lanes 5, 6). R3G (4−8 μM) displayed similar behavior; protection of the lower stem and the bulge was more pronounced with 8 μM R3G than with 20 μM R4K. Cleavages at C19−A20 in the lower stem as well as at G30 and G34 in the loop were observed (Figure 4A, lanes 7, 8). In the presence of GB4K (20 μM), no significant protection was observed. With 40 μM GB4K, U25 (bulge), U31, G33, and A35 (loop) as well as nucleotides 37−42 were partially protected, whereas the bands of A20, C30, and G34 were partially enhanced (Figure 4A, lanes 9, 10).

Uranyl Nitrate Photoprobing of TAR RNA (Figure 4B). UO_2^{2+} has high affinity to DNA and RNA backbone phosphates; irradiation of the uranyl−nucleic acid complex with light, at a wavelength of 420 nm, leads to the oxidation of a proximal deoxyribose/ribose ring, resulting in cleavage of the backbone *(41, 42, 56, 57)*. Slightly acidic conditions (pH 6.5 and lower) modulate the uranyl cleavage, reflecting the conformational changes of nucleic acids. For probing the conjugates' interactions with TAR RNA, the best results were obtained in cacodylate buffer, pH 6.5, 25−50 μM uranyl nitrate, and 10−20 min irradiation; 1 μM TAR was cleaved by 50 μM uranyl nitrate after 10 min irradiation, in an uneven manner. Nucleotides of the lower stem (C18−G21 and U40) and of the loop (U31 and G33) were better cleaved by the uranyl cation than those of the upper stem (G26−C29). The bulge (U25 and C24) was hypersensitive to cleavage (Figure 4B, lane 2).

In the presence of Tat R52 (4 μM), protection of the loop and the upper stem (A27−A35) as well as U38−G44 (the opposite strand) was observed, but no changes were observed in the bulge region. Cleavage at C18 and G21 was enhanced (Figure 4B, lanes 3, 4). With 10−20 μM R4K (Figure 4B, lanes 5, 6) and 4−8 μM R3G (Figure 4B, lanes 7, 8), the whole TAR RNA molecule appeared protected against cleavage. GB4K (20 μM), under the same conditions, did not affect TAR RNA uranyl photocleavage (Figure 4B, lane 9). 40 μM GB4K displayed protection of the upper stem (A27−C29), C39−G44 of the opposite strand, and the loop (C30−A35).

Lead Acetate Footprinting. Pb^{2+} cations cause cleavage predominantly of phosphoester bonds of RNA single-stranded regions. Cleavage also may occur in double-stranded regions if they contain weak, bulged, or destabilized base pairs *(58)*. Lead acetate footprinting was found to be a suitable and accurate method for the studies of AAC binding to TAR. In the presence of R52, A22−U40 and G26−C39 pairs were protected as well as C19, A20, A27, and G28 (Figure 4C, lanes 3, 4). Protection was also observed at G33 and G34 of the loop. In the presence of AAC, the protection of the bulge region with flanking base pairs was observed, along with some protection at G34 of the loop (Figure 4C, lanes 5−8). GB4K did not display any protection patterns in this experiment (Figure 4C, lanes 9, 10).

AAC Binding Sites on TAR RNA. All the gels were analyzed by densitometry using a "Storm 820" phosphoimager, and the intensities of the bands were determined by the ImageQuant program. The results of the measurements are presented in Figure 5 as the relative intensity of each band to the respective control band. The zero line stands for

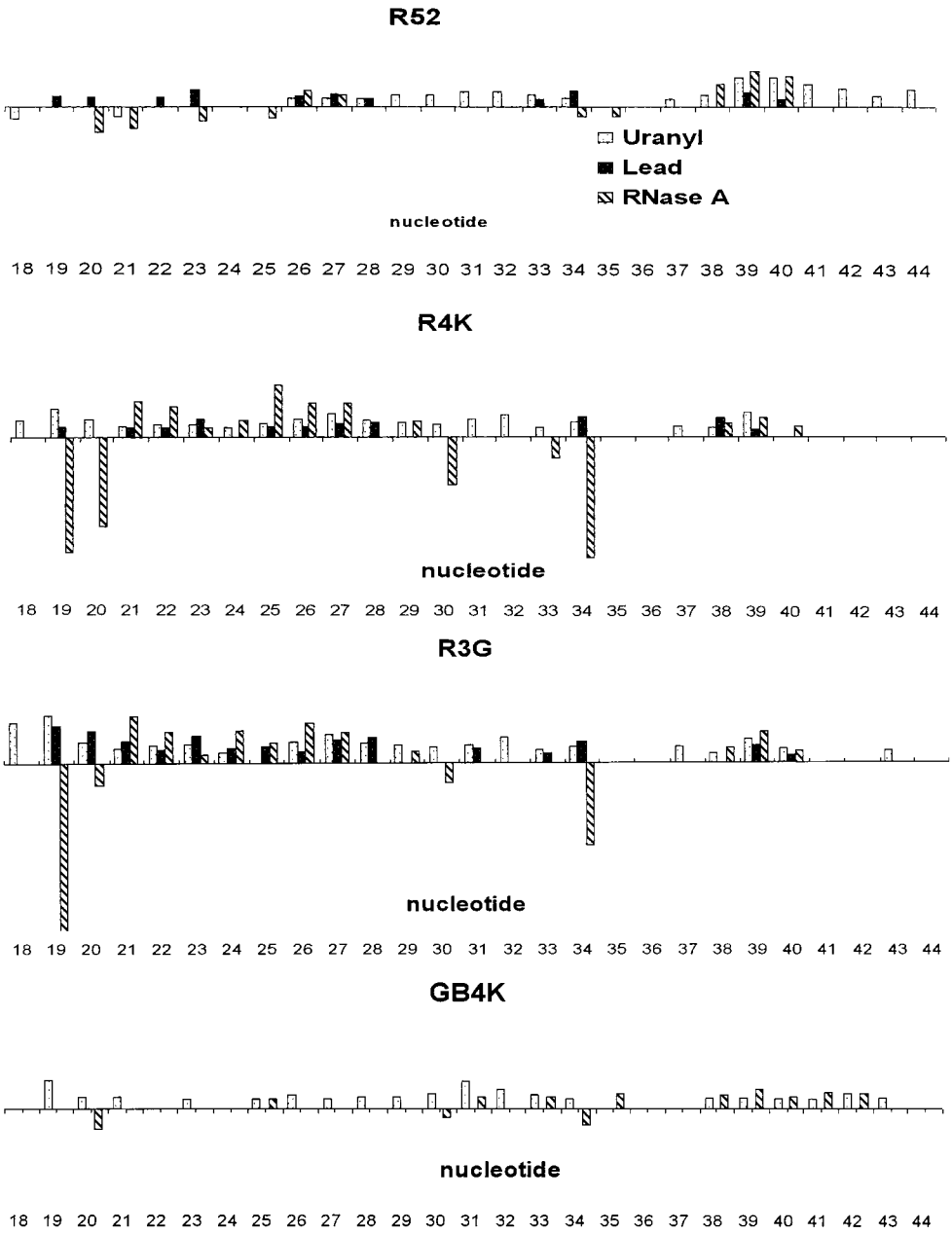

FIGURE 5: Summary of TAR RNA footprinting studies. The results are derived from densitometry of the gels presented in Figure 4. Bars represent percent of protection calculated for each band compared to "control" (in the absence of binders) in each method. Negative peaks stand for enhancement of cleavage at the nucleotide (mainly by RNase A). Lead acetate results allow accurate assignment of the binding site; RNase A mainly probes secondary structure changes, uranyl nitrate, at our conditions: low pH, probes both binding site and conformational changes.

the abscence of any effect (within 10% experimental error), positive peaks denote protection of the nucleotide from cleavage, and negative peaks represent cleavage enhancement (by RNase A) at certain positions due to conformational changes of TAR RNA. From these graphs, the binding sites for R52 and AAC were derived (Figure 6).

Specificity of Binding of AAC to TAR RNA. Binding of R3G and R4K to a variety of short RNA oligonucleotides, including rG_{15}, $rG_{15}-rC_{15}$ duplex, and truncated TAR RNA sequences, was tested by gel-shifts. The conjugates did not display any binding to these RNAs in the micromolar concentration range (data not shown). Binding competition experiments were performed with ^{32}P-labeled TAR RNA in the presence of various amounts of unlabeled yeast tRNA (Sigma). In gel-shift experiments, a 10-fold excess of tRNA did not inhibit complex formation between TAR and R52 or the conjugates (Figure 7 A,B). A 100-fold excess of tRNA inhibited complex formation (over 90% inhibition, data not shown). In the "single-hit" RNase A footprinting, the presence of a 10-fold excess of yeast tRNA in the reaction mixtures did not affect the protection pattern significantly. However, a trend of AAC binding inhibition to definite positions on TAR under these conditions was quite obvious (Figure 7C). Densitometry quantitations, as described above, showed these positions to be G21−U25, G28, and U38 (Figure 7D,E). Positions not affected by tRNA excess resemble the Tat R52 binding site (Figure 6, Figure 7E).

Metal Binding Sites on TAR RNA. The hypersensitivity of certain positions on TAR to cleavage by uranyl cation may reflect metal binding sites on TAR RNA *(41, 42, 57)*.

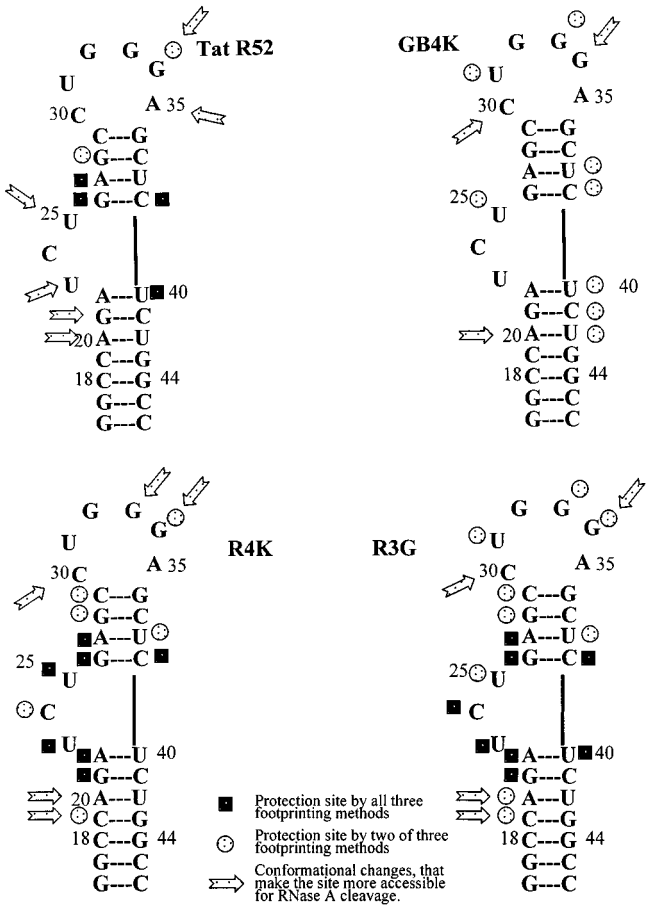

FIGURE 6: Schematic representation of Tat R52, R4K, R3G, and GB4K binding sites on TAR RNA. The results indicate that more than one molecule of R4K and R3G binds per one molecule of TAR. The high-affinity binding site, similar to that of Tat R52, is located in the bulge region. The low-affinity binding site is assigned to the loop−stem junction. GB4K binds TAR RNA inefficiently.

Thus, uranyl photocleavage experiments in the presence of divalent metal ions (Mg^{2+}, Ca^{2+}, and Co^{2+}) and citrate were performed (Figure 8 A,B). The presence of divalent metal salts (1 mM $MgCl_2$, $CaCl_2$, or $CoCl_2$) in the reaction inhibited the cleavage at the nucleotides G26, A27, and U30, whereas G33 and G34 gained increased sensitivity to uranyl (Figure 8A). Co^{2+} cation also protected G28 but did not affect the cleavage at G33 and G34, whereas Ca^{2+} protected U25 as well. At 37.5 μM citrate and 50 μM uranyl nitrate, G33 and G34 remained hypersensitive to cleavage, whereas cleavage at the rest of the nucleotides was inhibited (Figure 8B). Two tentative metal binding sites on TAR may thus be suggested: nucleotides G26 and A27 of the upper stem and near U30 of the loop. Another calcium cation may be coordinated in the bulge (U25). The cobalt cation is coordinated only at G26−A27 (and maybe involving G28). Hypersensitivity of G33−G34 to uranyl in the presence of citrate suggests a binding site for large cations, like UO_2^{2+}. Cleavage at this site is not affected by small cations, such as Mg^{2+}, Ca^{2+}, and Co^{2+} (Figure 8C,D).

Antiviral Activity of R3G and R4K. Equine infectious anemia virus (EIAV) of Wyoming strain is adapted to grow in equine dermal fibroblasts (ED), without damaging them with a titer of 1 pfu per cell (Malmquist virus) *(50)*. We used a significantly higher infection level (superinfection), around 10 pfu per cell, to accelerate the viral growth and to cause the development of the EIAV-induced cytopathic effect (cpe) in the cells at the late stage of the infection. In the absence of inhibitors, EIAV proliferated in the ED cells, reaching a plateau 9−12 days after infection (Figure 7). After 15−17 days, the viral titer in the medium dropped, and the cells appeared as cpe phenotype (Figure 8A,B): cell nuclei were condensed, vacuoles were observed in the cytoplasm, and the cells formed syncytia. Development of cpe started 10−12 days after infection, reaching a maximum on days 15−17, followed by rapid cell death and exfoliation from the plastic bottom of the well.

Addition of 50−100 μM R4K and 12.5−50 μM R3G to the EIAV-infected cells caused a significant (3−5-fold) inhibition of the viral growth in a dose-dependent manner (Figure 8). After day 12, a slight increase of the EIAV titer was observed. GB4K (100−250 μM) did not show any effect on viral growth. The toxicity of the conjugates for ED cells was tested by [^{3}H]thymidine incorporation as described previously *(47)*. The compounds, up to 1 mM concentration, did not inhibit DNA synthesis in the cells.

A noticeable inhibition of cpe development was observed at 25 and 50 μM R3G even after 13−15 days (Figure 9 C,D). Untreated cells at the same time displayed cpe development, whereas cells treated by R3G preserved the normal phenotype. This observation correlates with the viral production. Moreover, when R3G was added to the infected cells during the cpe onset (days 12−13), at day 15 the development of cpe was inhibited and cell damage was not noticeable. The viral titer decreased at least twice compared to control. At the same time, untreated cells developed massive cpe phenotype and were significantly damaged by day 15 (data not shown).

Intracellular Accumulation and Distribution of Fluorescent-Labeled Conjugates. Uptake of AAC by live cells and their intracellular distribution were described previously *(47)*. An R4K fluorescent derivative was prepared, and its uptake by rat neurons and human peripheral blood mononuclear cells was demonstrated. Similar experiments were performed using equine dermal fibroblasts, both uninfected and infected with EIAV. After 30−60 min incubation with 10 μg/mL either R4K-FITC or R3G-FITC, an intense fluorescence was observed in the cell nuclei (Figure 9B,D). This indicates that the conjugates efficiently penetrate into the ED cell nuclei of uninfected as well as infected cells.

DISCUSSION

Several approaches were used to create anti-TAR compounds as potential anti-HIV drugs. To date, a number of substances of various chemical nature were discovered in this field. Apart from peptide mimetics (as, e.g., *29*, *30*), these are, for example, DNA and PNA (peptide nucleic acid) antisense aptamers *(59, 60)*, PNA conjugates with arginine *(61)*, and naftalinimide and acridine−spermidine derivatives *(62)*.

Our concept of aminoglycoside−arginine conjugates as compounds that target TAR RNA has evolved from an idea of combination of the features of two types of molecules that bind RNA hairpin structures: arginine-rich peptides and aminoglycoside antibiotics.

Binding of Tat R52 Peptide and AAC to TAR RNA. NMR studies of aminoglycoside−RNA interactions *(33−35)* showed

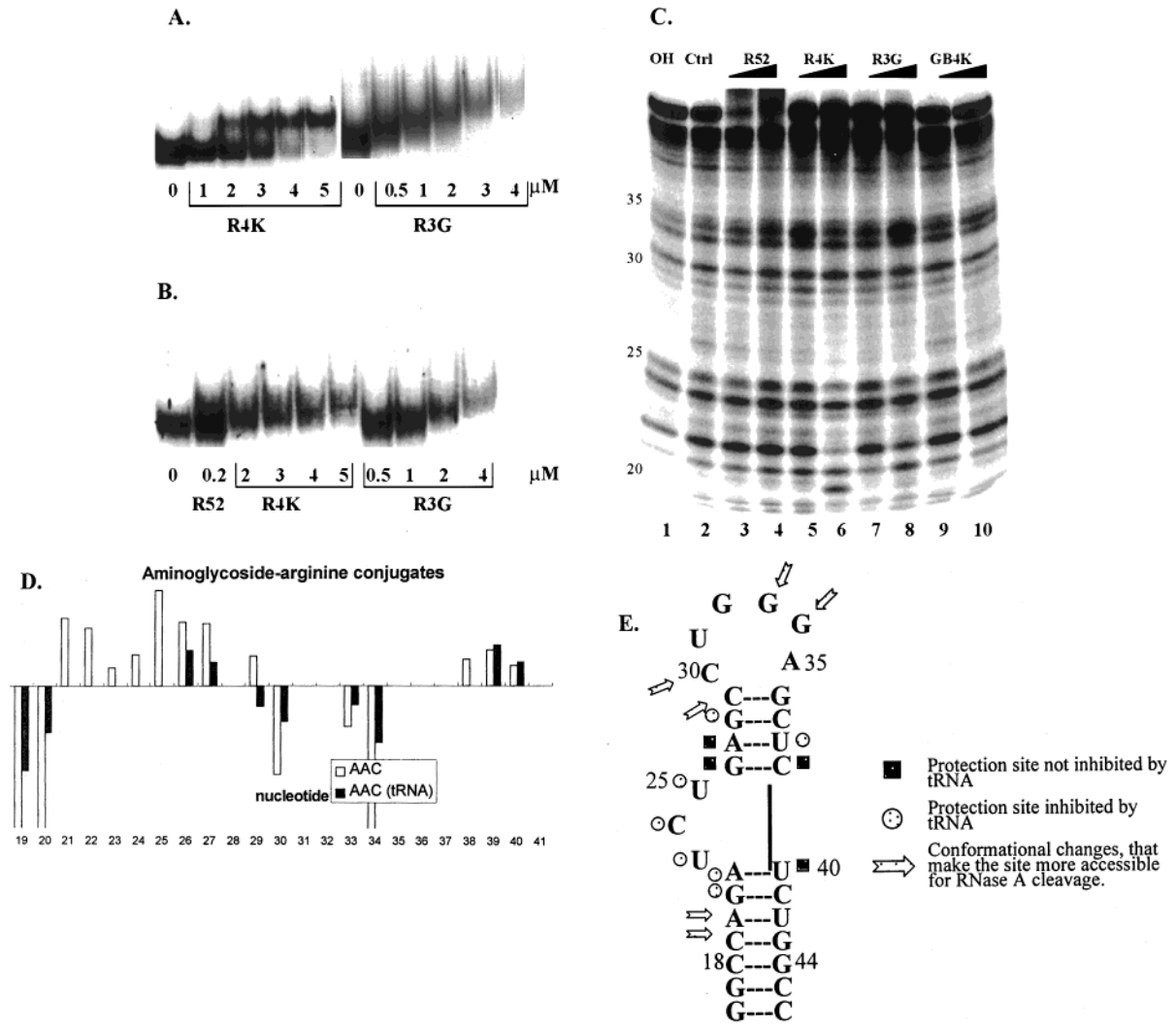

FIGURE 7: Effect of yeast tRNA on TAR RNA band shifts and RNase A footprinting in the presence of Tat R52, R3G, and R4K. (A) Band shifts of TAR RNA induced by binding of R4K and R3G (reproduced from ref *47*). 20 μL samples containing 10−12 nM ^{32}P-labeled TAR RNA and 1−5 μM R4K or 0.5−4 μM R3G in 10 mM Tris-HCl (pH 7.5) buffer, containing 70 mM NaCl, 0.2 mM EDTA, and 5% glycerol, were incubated for 10 min at 0 °C. Following the incubation, the samples were analyzed by electrophoresis on 10% native polyacrylamide gels (40:1). Gels were dried and visualized by autoradiography. R4K (left) forms 2:1 complexes with TAR RNA. R3G (right) forms complexes of increased molecular weight, and caused precipitation of TAR RNA in the wells (not shown). (B) Band shift of TAR complexes with R52, R4K, and R3G in the presence of an excess of yeast tRNA. 100 ng of yeast tRNA per lane does not inhibit the binding of Tat R52, R4K, and R3G to TAR RNA. Band shifts suggest one molecule of aminoglycoside−arginine conjugate per one molecule of TAR RNA in the complex. In the presence of 1 μg of tRNA per sample, the binding of *both* R52 and the conjugates was 90% inhibited. (C) In the presence of 0.5 μg of yeast tRNA, the RNase A footprinting of TAR complexes with R52, R4K, R3G, and GB4K has a similar pattern as seen in Figure 4. Binding of AAC to the low-affinity binding site on TAR is partially supressed. (D) Qantitation of band intensities of lane 5 of the gel, presented in panel C, in comparison to lane 5 of Figure 4A. (E) Schematic representation of AAC binding to TAR RNA in the presence of excess of tRNA.

that the antibiotics bind preferentially at the junctions between single- and double-stranded regions on the RNA. Since there are two such regions on TAR RNA (between the upper stem and the loop and between the lower stem and the bulge), it was of interest to investigate whether aminoglycoside−arginine conjugates would inherit the aminoglycoside binding pattern.

Based on the footprinting results (Figures 4−6), we can suggest that R52 makes contacts with TAR at the G26−C39 pair, the base pair that was determined to be crucial for TAR major groove recognition by ligands *(63)*; contacts with A27, G28, and G40 were also assigned. The whole region between the bulge and the loop acquires a certain buried conformation (as can be concluded from uranyl footprinting results). Binding of R52 causes conformational changes in the bulge, making U23 and U25 as well as A20 and G21 more accessible to RNase A cleavage. In the loop, G34 and A35 become more exposed to RNase digestion, whereas in uranyl and lead footprinting experiments, G34 is found to be protected. G34−G33, shown later on, is a metal binding site. The results of our footprinting experiments suggest that the binding site for R52 (Figure 6) is similar to that for Tat peptide *(27)* and in accordance with a model of Tat peptide−TAR RNA complex *(64)*.

The binding of AAC to TAR differs significantly from R52 binding, while R4K and R3G bind similarly to TAR (Figures 4−6). The contacts with TAR can be assigned at the A22−U40, G26−C39, and A27−U38 pairs (A27 with R4K) as well as at G21. The whole bulge region in each case is involved in the binding. C19 and A20 (with R3G) are protected in UO_2^{2+} and Pb^{2+} footprinting exeriments, while they are readily cleaved by RNase A. C30, U31 (only

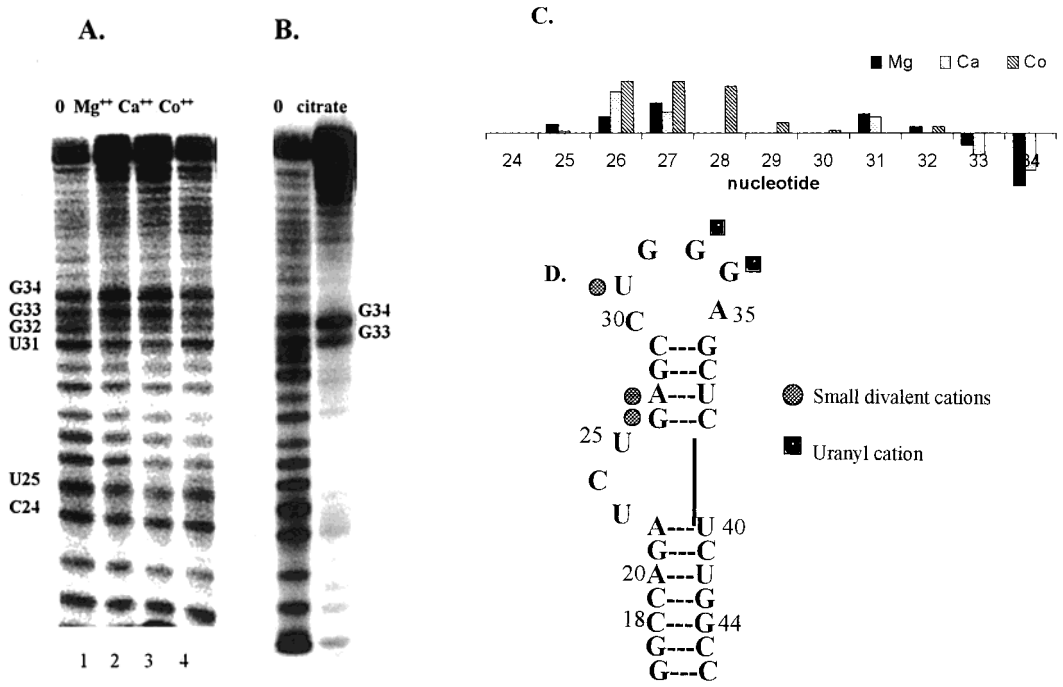

FIGURE 8: (A) Uranyl photocleavage of TAR RNA in the presence of divalent metal ions. Around 100 nM 5′-^{32}P end-labeled TAR was cleaved by 50 μM uranyl nitrate. The samples were irradiated at 420 nm for 20 min. Lane 1, cleavage in the absence of metal ions; lane 2, 1 mM $MgCl_2$; lane 3, 1 mM $CaCl_2$; lane 4, 1 mM $CoCl_2$. (B) Uranyl photocleavage of TAR RNA in the presence of citrate. Around 100 nM 5′-^{32}P-labeled TAR was cleaved by 50 μM uranyl nitrate in the presence of 37.5 μM citrate. Nucleotides G33 and G34 remain hypersensitive to uranyl, while cleavage at the other sites is inhibited by citrate. (C) Quantitation of the gel band intensities, presented in panel A. (D) Schematic representation of metal cation binding sites on TAR RNA.

with R3G), G33 (only with R4K), and G34 are more exposed to RNase A digestion upon AAC binding, whereas in uranyl and lead footprinting, there is protection at G34 with both compounds. This behavior resembles R52 binding to TAR. Molecular weights of AACs are smaller than that of R52, and, assuming R52 is folded as β-hairpin, similar to the described model of Tat basic nonapeptide bound to TAR *(64)*, we can suggest that AACs occupy approximately two-thirds of the peptide molecular volume. AACs make more contacts with TAR than R52 (Figure 6); thus, it is plausible that there are two molecules of AAC in the complex with TAR RNA. This suggestion is supported by the gel-shifts and the fact that the whole TAR RNA molecule in the presence of AAC is protected against UO_2^{2+} cleavage (uranyl footprinting under our conditions reflects conformational changes in RNA). In contrast, upon R52 binding, only the upper stem part of TAR is protected. There is a certain similarity in AAC protection of TAR RNA to that of neomycin B, which protects the C19−G43 and A22−U40 pairs of the lower stem, U23 and U25 of the bulge, and G26 of the upper stem *(37)*. Thus, we can conclude that AACs possess both aminoglycoside-like and peptide-like features of binding to TAR. We suggest that one of the AAC molecules binds in the lower stem−bulge region, whereas the second one binds in the upper stem, similarly to R52, but inducing different conformational changes in the TAR RNA loop (Figure 6).

It was unexpected that GB4K, which is very similar to R4K (Figures 1 and 2), differs so drastically in TAR RNA binding. GB4K is a very weak TAR RNA binder and presumably forms only nonspecific electrostatic contacts with TAR. Nevertheless, in the presence of GB4K, U38−U42 are found to be protected as well as U25, U31, and G33. Conformational changes upon GB4K binding in TAR, similarly to AAC, induce cleavages by RNase A at A20, C30, and G34, which is probably a general feature of binding of this class of ligands to TAR RNA (Figure 6). We conclude that in the context of aminoglycoside-based peptidomimetic TAR binders, not any guanidine-bearing side chains are suitable for the efficient recognition; so far, only arginine residues were properly recognized by TAR RNA. It is worth noting that streptomycin, bearing two guanidino groups on the deoxystreptamine ring, binds to TAR *(37)*, but is not an efficient inhibitor of the Tat−TAR interaction *(36)*. Apparently, the linker between the "core" and the "headgroup" (Figure 1) is very important for RNA binding. We suggest that the α-amino groups of the conjugated arginine moieties are essential for this interaction.

Specificity of AAC Binding to TAR. The conjugates bind to TAR RNA with high affinity, but not to a variety of short RNA oligonucleotides and truncated TAR RNA sequences (in the micromolar concentration range). No lower than a 100-fold excess (i.e., 10-fold) of tRNA inhibits AAC−TAR complex formation, similar to the effect of tRNA on Tat-derived peptide binding to TAR *(37)*. This demonstrates similar specificity of the binding of Tat R52 and AAC to TAR RNA.

Previously, we suggested that TAR forms the complex with two molecules of R4K (Figure 7A, *47*). The difference in band shifts in the presence of tRNA (Figure 7B) may indicate that the TAR−R4K complex, under this condition, contains only one molecule of R4K. The same may be true for the R3G−TAR complex, whose band shifts are more complicated for interpretation, since R3G is a mixture of isomers. These observations support our suggestion that R4K

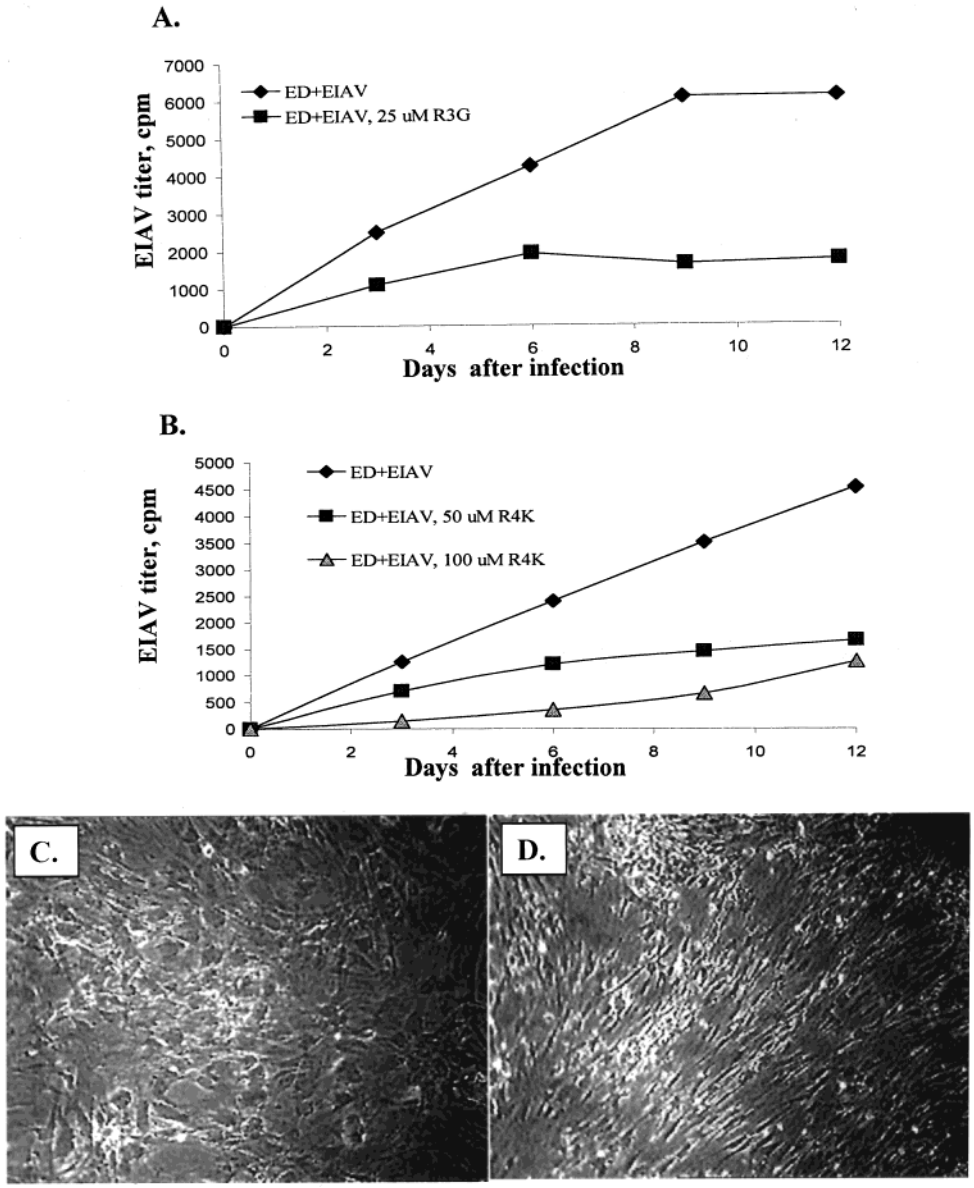

FIGURE 9: (A, B) Effect of R3G (A) and R4K (B) on EIAV replication in ED cells. The cells were infected with 10 pfu of EIAV per cell (superinfection) and were cultured in the medium, supplemented with [^{3}H]uridine. R3G and R4K were added to the medium in a range of 12.5−100 μM. Viral titer was assayed every 3 days by radioactive uridine incorporation in the RNA of the viral particles. Each data point represent averages of 6 (R3G) and 4 (R4K) experiments (variation within 10%). R3G inhibited the viral growth at 12.5 and 25 μM; R4K, at 50 and 100 μM. (C, D) Optical microscopy of the cpe development in EIAV-infected ED cells in the presence of R3G. The images were taken with an Axiovert 100M (Zeiss) microscope using a 40× planar objective. (C) After 13−15 days, EIAV-infected ED cells started to form syncytia, that indicates the onset of the EIAV cytopathic effect (cpe). (D) The cells treated with 25 μM R3G preserve normal fibroblast phenotype on the same day of infection.

and R3G bind to at least two sites on TAR RNA, which are different in affinity. These sites could be distinguished by RNase A footprinting in the presence of an excess of tRNA. The AAC protection pattern in the presence of tRNA tends to be similar to that of R52, while the protection of G21−U25 was inhibited (Figure 7D). The site with higher affinity involves the bulge and the flanking base pairs, similar to the Tat peptide (like R52) binding site, while the low-affinity site is in the lower stem−bulge region, similar to the neomycin B binding site (Figure 7E, Figure 11). It is worth noting that 1D NMR spectra taken at different ratios of R4K to TAR suggest that R4K preferentially binds first to one and then to the second site on TAR (in collaboration with Professor T. L. James, UCSF, unpublished results).

GB4K displays a weak interaction with TAR that does not involve the specific site. In contrast to R4K and R3G, the GB4K−TAR interaction is completely inhibited by tRNA.

Metal Binding Sites on TAR RNA. The bulge and loop regions of TAR are hypersensitive to uranyl-induced degradation. A reasonable explanation of this phenomenon could be that the bulge is a metal binding site (e.g., for Mg^{2+}), as was indicated previously *(45, 46)*, and UO_2^{2+} readily binds to this region. Four Ca^{2+} ions were found in the X-ray structure of model TAR RNA, which contains all the correct sequence of wild-type TAR 18−44 and is lacking the loop *(43)*. One of these calcium ions makes contacts with phosphate oxygens of U23, C24, and G26, and also interacts with A22 through a water molecule. Two other Ca^{2+} ions make one direct contact with the RNA (G26 and A27, respectively). The fourth calcium ion participates in interactions with the bases of G21, A22, and G26.

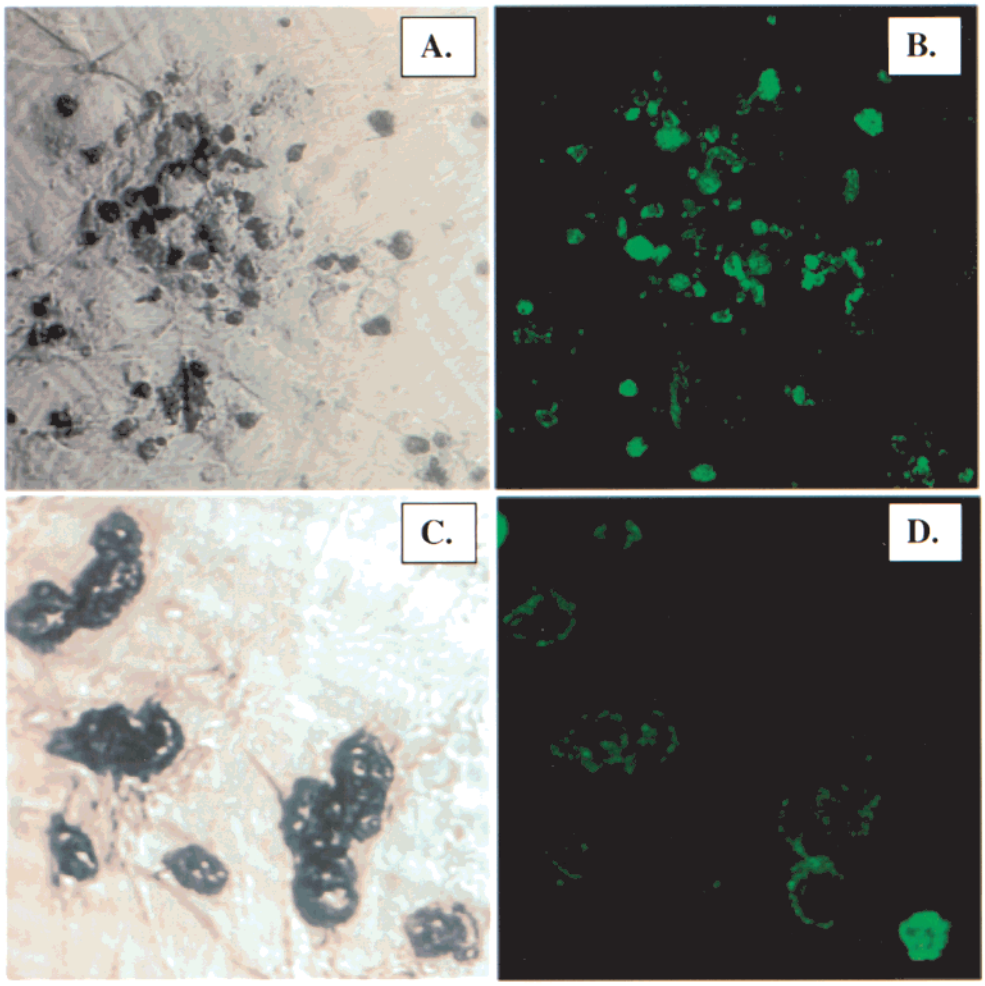

FIGURE 10: Confocal microscopy images of live EIAV-infected ED cells stained with R3G-FITC. The images were taken with an Axiovert 100M (Zeiss) microscope using a 63× water immersion objective. (A) Optical microscopy of EIAV-infected ED cells, on day 16. The cells are significantly damaged. (B) The same fields, confocal fluorescent microscopy at 488 nm excitation. Fluorescent R3G derivative, R3G-FITC, accumulates in the cell nuclei. (C and D) Same as (A) and (B) at higher magnification (digital, 8×).

Uranyl photocleavage of TAR RNA in the presence Mg^{2+}, Ca^{2+}, and Co^{2+} suggests the binding sites for divalent metal cations at positions G26 and A27 as well as U31−G32 (Mg^{2+} and Ca^{2+}). Another binding site for UO_2^{2+} is located in the loop (G33−G34). In the presence of Mg^{2+} and Ca^{2+}, cleavage at these nucleotides by uranyl is enhanced (Figure 8A). We can conclude that metal binding to TAR in solution is generally similar to the crystallization conditions *(43)*. G26−A27 is probably the metal (Mg^{2+}) binding site. G33−G34 may bind some cation other than Mg^{2+} or Ca^{2+} (Figure 8D, Figure 11). Since G26 and A27 are part of the Tat binding site, it is plausible that metals (especially Mg^{2+}) are structurally important for Tat−TAR interaction whereas metals bound in the TAR loop may contribute to the interaction with cyclin T1.

Antiviral Activity of the Aminoglycoside−Arginine Conjugates. A homology between EIAV and HIV transcription activation mechanisms allowed us to use EIAV-infected cells as a model of HIV infection. It was recently shown that EIAV Tat and equine cyclin T1 form a protein complex that specifically binds to EIAV TAR, which indicates that highly divergent lentiviral Tat proteins activate transcription from their cognate LTR promoters by essentially identical mechanisms *(65)*. The conception of "minimal lentiviral Tat" *(66)*, which consists of only core and basic domains, allowed us to use AAC, Tat basic domain mimetics, as inhibitors of EIAV proliferation.

The conjugates caused pronounced inhibition of EIAV proliferation in cell culture at 100 μM R4K and 25−50 μM R3G. The compounds were not toxic to the cells up to 1 mM. The antiviral activities of the conjugates correspond well to the K_d's of their complexes with TAR RNA, measured by gel-shifts [83 nM for R3G and 416 nM for R4K *(47)*]. GB4K did not display any activity in cell culture, which is in accordance with the absence of its binding to TAR in vitro. The cytopathic effect of the virus on equine fibroblasts was efficiently inhibited by R3G, which correlated with viral growth suppression. Even at the relatively late infection period, addition of R3G suppressed EIAV proliferation and the development of cpe.

FITC-labeled conjugates accumulated in the infected equine fibroblast nuclei from a dilute solution that suggests the active transport of the conjugates into the cells.

In a collaborative study *(67)*, it was found that R4K and R3G inhibit HIV-1 NL4-3 replication at EC_{50} values of 15 and 30 μM for R3G and R4K, respectively, which correlates with their affinity to TAR RNA and their anti-EIAV activity. No detectable toxicity of R3G and R4K to MT-4 cells was

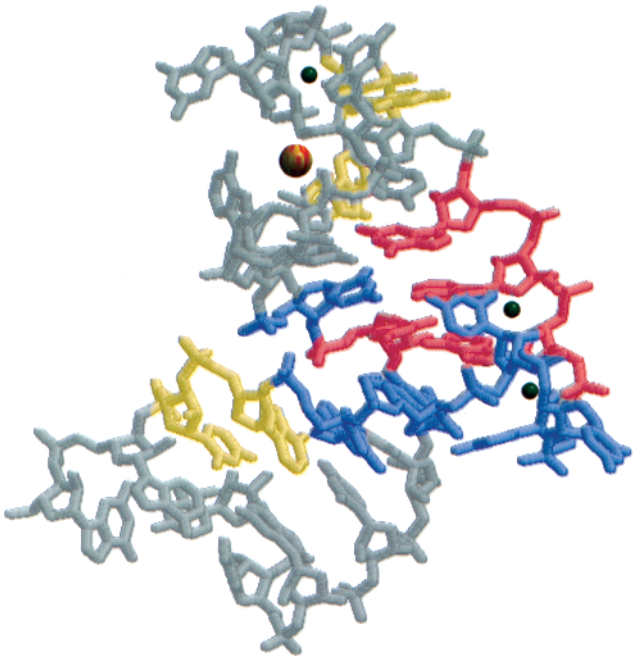

FIGURE 11: Schematic representation of aminoglycoside−arginine conjugate (AAC) binding sites on TAR RNA. The NMR average structure of TAR RNA complex with arginine amide was obtained from the Protein Data Bank, access code 1arj. Only the nucleic acid chain is presented. Nucleotides highlighted in pink represent high-affinity binding sites for AAC and Tat peptide. Binding of AAC to this site is not inhibited by excess tRNA. Nucleotides highlighted in blue represent low-affinity binding sites for AAC and aminoglycosides (e.g., neomycin B). Binding of AAC to this site is inhibited by a 10-fold excess of tRNA. Nucleotides highlighted in yellow represent sites of major conformational changes induced by AAC binding to TAR. These positions are cleaved by RNase A in the TAR−AAC complex, but are not cleaved in the absence of AAC. Small green balls represent proposed Mg^{2+} and Ca^{2+} binding sites. The big yellow ball represents the UO_2^{2+} binding site.

observed at concentrations higher than 1000 μM and around 4000 μM, respectively *(67)*. Both compounds also inhibited the binding of a monoclonal antibody (12G5) directed to CXC chemokine receptor (CXCR4), as well as the intracellular Ca^{2+} signal induced by stromal cell-derived factor SDF-1α on CXCR4-positive cells or peripheral blood mononuclear cells. This suggests an interaction of AAC with CXCR4, the coreceptor used by T-tropic, X4 strains of HIV-1. GB4K failed to display any anti-HIV activity or CXCR4 antagonist activity. Unlike SDF-1α and R4K, R3G inhibited the binding of HIV-1 NL4-3 to MT-4 cells. It was suggested that AACs inhibit HIV replication through a bimodal action: blockade of CXCR4 and inhibition of virus binding to cells *(67)*. A similar type of action could not be assigned to their anti-EIAV activity, since the Malmquist derivative of Wyoming strain, used in the present study, is avirulent and is incapable of directly infecting equine fibroblasts *(50)*.

Conclusion. Aminoglycoside−arginine conjugates, described in this report, are small molecules (molecular mass ~1000 Da) able to mimic the binding of Tat peptide to TAR. Despite being only model compounds, the conjugates reveal high affinity and specificity of TAR RNA binding, very low cytotoxicity, and antilentiviral potency. We hope that the ideology described in this article will help to create anti-HIV drugs with high selectivity, specificity, and activity as well as low toxicity.

ACKNOWLEDGMENT

We gratefully acknowledge the help and advice of Professors A. Yaniv and A. Gazit (Sackler Medical School, Tel-Aviv University). We thank Mr. V. Tougarinov (Structural Biology, WIS) for help in 2D NMR studies; Dr. E. Korkotian (Brain Research, WIS) for help in the confocal microscopy studies; Dr. S. Weinstein and Mrs. M. Laschever (Structural Biology, WIS) for their kind permission to use their laboratory facilities.

REFERENCES

1. Gait, M. J., and Karn, J. (1995) *Trends Biotechnol. 13*, 430−438.
2. Calnan, B. J., Tidor, B., Biancalana, S., Hudson, D., and Frankel, A. D. (1991) *Science 252*, 1167−1171.
3. Kingsmann, S. M., and Kingsmann, A. J. (1996) *Eur. J. Biochem. 240*, 491−507.
4. Cullen, B. R. (1998) *Cell 93*, 685−692.
5. Weeks, K. M., Ampe, C., Schultz, S. C., Steitz, T. A., and Crothers, D. M. (1990) *Science 249*, 1281−1285.
6. Cordingley, M. G., LaFemina, R. L., Callahan, P. L., Condra J. H., Sardana, V. V., Graham, D. J., Nguyen, T. M., LeGrow, K., Gotlib, L., Schalabach, A. J., and Colonno, R. J. (1990) *Proc. Natl. Acad. Sci. U.S.A. 87*, 8985−8989.
7. Dingwall, C., Ernberg, I., Gait, M. J., Green, S. M., Heaphy, S., Karn, J., Lowe, A. D., Singh, M., and Skinner, M. A. (1990) *EMBO J. 9*, 4145−4153.
8. Calnan, B. J., Biancalana, S., Hudson, D., and Frankel, A. D. (1991) *Genes Dev. 5*, 201−210.
9. Weeks, K. M., and Crothers, D. M. (1991) *Cell 66*, 577−588.
10. Weeks, K. M., and Crothers, D. M. (1992) *Biochemistry 31*, 10281−10287.
11. Churcher, M. J., Lamont, C., Hamy, F., Dingwall, C., Green, S. M., Lowe, A. D., Butler, P. J. G., Gait, M. J., and Karn J. (1993) *J. Mol. Biol. 230*, 90−110.
12. Long, K. S., and Crothers, D. M. (1995) *Biochemistry 34*, 8885−8895.
13. Dingwall, C., Ernberg, I., Gait, M. J., Green, S. M., Heaphy, S., Karn, J., Lowe, A. D., Singh, M., Skinnre, M. A., and Valerio, R. (1989) *Proc. Natl. Acad. Sci. U.S.A. 86*, 6925−6929.
14. Roy, S., Delling, U., Chen, C.-H., Rosen, C. A., and Sonnenberg, N. (1990) *Genes Dev. 4*, 1365−1373.
15. Delling, U., Reid, L. S., Barnett, R. W., Ma, M. Y.-X., Climie, S., Sumner-Smith, M., and Sonnenberg, N. (1992) *J. Virol. 66*, 3018−3025.
16. Rana, T. M., and Jeang, K.-T. (1999) *Arch. Biochem. Biophys. 365*, 175−185.
17. Wei, P., Garber, M. E., Fang, S.-M., Fischer, W. H., and Jones, K. A. (1998) *Cell 92*, 451−462.
18. Puglisi, J. D., Tan, R., Calnan, B. J., Frankel, A. D., and Williamson, J. R. (1992) *Science 257*, 76−80.
19. Puglisi, J. D., Chen, L., Frankel, A. D., and Williamson, J. R. (1993) *Proc. Natl. Acad. Sci. U.S.A. 90*, 3680−3684.
20. Puglisi, J. D., Chen, L., Blanchard, S., and Frankel, A. D. (1995) *Science 270*. 1200−1203.
21. Aboul-Ela, F., Karn, J., and Varani, G. (1995) *J. Mol. Biol. 253*, 313−332.
22. Ye, X., Kumar, R. A., and Patel, D. J. (1995) *Chem. Biol. 2*, 827−840.
23. Aboul-Ela, F., Karn, J., and Varani, G. (1996) *Nucleic Acids Res. 24*, 3974−3981.
24. Brodsky, A. S., and Williamson, J. R. (1997) *J. Mol. Biol. 267*, 624−639.
25. Mujeeb, A., Bishop, K., Peterlin, B. M., Truck, C., Parslow, T. G., and James, T. L. (1994) *Proc. Natl. Acad. Sci. U.S.A. 91*, 8248−8252.
26. Mujeeb, A., Parslow, T. G., Yuan, Y. C., and James, T. L. (1996) *J. Biomol. Struct. Dyn. 13*, 649−661.

27. Huq, I., and Rana, T. M. (1997) *Biochemistry 36*, 12592−12599.
28. Huq, I., Tamilarasu, N., and Rana, T. M. (1999) *Nucleic Acids Res. 27*, 1084−1093.
29. O'Brien, W. A., Sumner-Smith, M., Mao, S.-H., Sadeghi, S., Zhao, J.-Q., and Chen, I. S. Y. (1996) *J. Virol. 70*, 2825−2831.
30. Hamy, F., Felder, E. R., Heizmann, G., Lazdins, J., Aboul-Ela, F., Varani, G., Karn, J., and Klimkait, T. (1997) *Proc. Natl. Acad. Sci. U.S.A. 94*, 3548−3553.
31. Huq, I., Wang, X., and Rana, T. M. (1997) *Nat. Struct. Biol. 4*, 881−882.
32. Huq, I., Ping, Y.-H., Tamilarasu, N., and Rana, T. M. (1999) *Biochemistry 38*, 5172−5177.
33. Jiang, L., Suri, A. K., Fiala, R., and Patel, D. J. (1996) *Chem. Biol. 4*, 35−50.
34. Fourmy, D., Yoshizawa, S., and Puglisi, J. D. (1998) *J. Mol. Biol. 277*, 333−345.
35. Fourmy, D., Recht, M. I., and Puglisi, J. D. (1998) *J. Mol. Biol. 277*, 347−362.
36. Zapp, M. L., Stern, S., and Green, M. R. (1993) *Cell 74*, 969−978.
37. Mei, H.-Y., Galan, A. A., Halim, N. S., Mack, D. P., Moreland, D. W., Sanders, K. B., Truong, H. N., and Czarnik, A. W. (1995) *Bioorg. Med. Chem. Lett. 5*, 2755−2760.
38. Wang, S., Huber, P. W., Mei, C., Czarnik, A., and Mei, H.-Y. (1998) *Biochemistry 37*, 5549−5557.
39. Mei, H.-Y., Mei, C., Heldsinger, A., Lemrow, S. M., Loo, J. A., Sannes-Lowery K. A., Sharmeen, L., and Czarnik A. W. (1998) *Biochemistry 37*, 14204−14212.
40. Hermann, T., Westhof, E. (1999) *J. Med. Chem. 42*, 1250−1261.
41. Bassi, G. S., Mollegaard, N.-E., Murchie, A. I. H., von Kitzing, E., and Lilley, D. M. J. (1995) *Nat. Struct. Biol. 2*, 45−55.
42. Bassi, G. S., Mollegaard, N. E., Murchie, A. I. H., and Lilley, D. M. J. (1999) *Biochemistry 38*, 3345−3354.
43. Clouet-d'Orval, B., Stage, T. K., and Uhlenbeck, O. C., (1995) *Biochemistry 34*, 11186−11190.
44. Ippolito, J. A., and Steitz, T. A. (1998) *Proc. Natl. Acad. Sci. U.S.A. 95*, 9819−9824.
45. Zachairas, M., and Hagerman, P. J. (1995) *J. Mol. Biol. 247*, 486-500.
46. Zacharias, M., and Hagerman, P. J. (1995) *Proc. Natl. Acad. Sci. U.S.A. 92*, 6052−6056.
47. Litovchick, A., Evdokimov, A. G., and Lapidot, A. (1999) *FEBS Lett. 445*, 73−79.
48. Lapidot, A., Litovchick, A., and Evdokimov, A. G. (1998) Israeli Patent 127773.
49. Scaringe, S. A., Wincott, F. E., and Caruthers, M. H. (1998) *J. Am. Chem. Soc. 120*, 11820−11821.
50. Malmquist, W. A., Barnett, D., and Becvar, C. S. (1973*) Arch. Gesamte Virusforsch. 42*, 361−370.
51. Carpenter, S., and Chesebro, B. (1989) *J. Virol. 63*, 2492−2496.
52. Cheevers, W. P., Archer, B. G., and Crawford, T. B. (1977) *J. Virol. 24*, 489−497.
53. Cooper, D. J., Ydis, M. D., Marigliano, H. M., and Traubel, T. (1971) *J. Chem. Soc. C60*, 2876−2882.
54. Davis, D. G., and Bax, A. (1985) *J. Am. Chem. Soc. 107*, 2820−2826.
55. Dabrowiak, J. C., Goodisman, J., and Ward, B. (1997) in *Drug−DNA Interaction Protocols* (Fox, K. R., Ed.) pp 23−42, Humana Press Inc., Totowa, NJ.
56. Nielsen, P. E., Hiort, C., Sonnichsen, S. H., Buchard, O., Dahl, O., and Norden, B. (1992) *J. Am. Chem. Soc. 114*, 4967−4975.
57. Mollegaard, N. E., Murchie, A. I. H., Lilley, D. M. J., and Nielsen, P. E. (1994) *EMBO J. 13*, 1508−1513.
58. Wallis, M. G., Streicher, B., Wank, H., von Ahsen, U., Clodi, E., Wallace, S. T., Famulok, M., and Schroeder, R. (1997) *Chem. Biol. 4*, 357−366.
59. Boiziau, C., Dausse, E., Yurchenko, L., and Toulme, J.-J. (1999) *J. Biol. Chem. 274*, 12730−12737.
60. Boulme, F., Freund, F., Moreau, S., Nielsen, P., Gryaznov, S., Toulme, J.-J., and Litvak, S. (1998) *Nucleic Acids Res. 26*, 5492−5500.
61. Di Giorgio, A. F., Pairot, S., Patino, N., Condom, R., Di Giorgie, C., Aumelas, A., Aubertin, A.-M., and Guedj, R. (1999) *Nucleosides Nucleotides 18*, 263−275.
62. Hamy, F., Brodani, V., Florsheimer, A., Stark, W., Blommers, M. J. J., and Klimkait, T. (1998) *Biochemistry 37*, 5086−5095.
63. Gelus, N., Hamy, F., and Bailly, C. (1999) *Bioorg. Med. Chem. 6*, 1075−1079.
64. Seewald, M. J., Metzger, A. U., Willbold, D., Rosch, P., and Sticht, H. (1998) *J. Biomol. Struct. Dyn. 16*, 683−692.
65. Bieniasz, P. D., Grdina, T. A., Bogerd, H. P., and Cullen, B. R. (1999) *Mol. Cell. Biol. 19*, 4592−4599.
66. Derse, D., Carvalho, M., Carrol, R., and Peterlin, B. M. (1991) *J. Virol. 65*, 7012−7015.
67. Cabrera C., Gutierrez A., Blanco J., Barretina J., Litovchick A., Lapidot A., Evdokimov A. G., Clotet B., and Este J. A. (1999) *AIDS Res. Human Retrovir.* (submitted for publication).

BI9917885